ULTRASONIC PULSATING WATER JET DRILLING-PRELIMINARY STUDY

GABRIEL STOLARIK[1], AKASH NAG[2], DAGMAR KLICHOVA[3], SERGEJ HLOCH[3]

[1]Faculty of Manufacturing Technologies TUKE with a seat in Presov, Slovak Republic

[2]VSB - Technical University of Ostrava, Ostrava, Czech Republic

[3]The Czech Academy of Sciences, Institute of Geonics, Czech Republic

DOI: 10.17973/MMSJ.2025_03_2025005

e-mail to corresponding author: gabriel.stolarik@tuke.sk

This study presents pioneering experiments utilizing an ultrasonic pulsating water jet (PWJ) for drilling into aluminum alloy 5.5 mm thick following a circular trajectory with a diameter of 6 mm. The innovative approach combines the high frequency of water pulses with frequency of 20 kHz impinging the surface of material at Bernoulli impact speed was 254 m/s to enhance drilling efficiency and observe drilling precision. Circular trajectories with 10, 15 and 20x transition provided basic information on the characterization of the erosion process and the factors entering the process. Finally, an 80x multiple repetition confirmed the complete cutting of the sample and the separation of the core material from the surrounding material. The research provides a foundational understanding of UPWJ technology's potential applications in environmentally clean manufacturing processes.

KEYWORDS

ultrasonic pulsating water jet, circular erosion milling, erosion drilling, sustainability

1 INTRODUCTION

Water droplet erosion is generally perceived as an undesirable natural phenomenon discovered on technical devices such as steam turbines in the early 20th century (Cook, 1928). Water droplet erosion occurs when water droplets impinge the surface with a high velocity, causing localized deformation following material removal (Field, 1999). The mechanism involves the initial impact creating a high-pressure shock wave, followed by the propagation of stress waves within the material (Hancox & Brunton, 1966). Periodically or non-periodically repeated impacts lead to the formation of micro-cracks, material fatigue, and surface integrity degradation (Marzbali et al., 2023). From a temporal perspective, erosion evolution is divided into basic stages based on boundary conditions: incubation, accumulation and terminal (Gujba et al., 2016). As erosion progresses to advanced stages, the rate of material removal can attenuate due to the formation of surface with stochastically created artefacts changing in the material's microstructure and topography (Poloprudsky et al., 2024). Understanding this attenuation is crucial for optimizing erosion-based processes and extending the lifespan of materials subjected to erosive environments (Hloch et al., 2024). Although the mechanism is still not sufficiently understood due to phenomena that we do not yet understand (Fujisawa, 2023), the accumulated knowledge (Vijay et al., 2018) in conjunction with the use of robotic devices allows the use of water droplets as a new technological tool for different purposes. These applications include surface treatment techniques (Siahpour et al., 2023) such as peening (Srivastava et al., 2022; Stolárik et al., 2024), surface modification methods like roughening (Stolárik et al., 2023), and the investigation of erosion resistance in various ductile (Mann & Arya, 2003) and non-metallic materials. All these methods can be technologically executed using clean water in form of water droplets, ensuring an environmentally friendly operation without any undesirable side effects (Nastic et al., 2023). Additionally, there is an increasing demand for using an abrasive-less water jet, which maintains the characteristics of a cold tool while simplifying the equipment needed for abrasive delivery logistics and minimizing the risk of machined surface contamination from abrasive artefacts (Arola & McCain, 2000). The necessity of using an abrasive-less water jet, which utilizes water droplets at very low pressures, arises from the need to minimize damage while achieving precise material removal (Szada-Borzyszkowska et al., 2024). This approach reduces the risk of excessive wear and tear, making it suitable for delicate or high-precision applications. The process can be utilised in the medical industry for micro-machining or precision machining of surgical instruments, drilling of precision holes in composite materials used in aircraft parts, drilling in circuit boards without thermal damage, and finally in artistic sculptures and detailed engraving. Despite the advancements in understanding water droplet erosion, a significant research gap remains in optimizing the parameters for ultrasonic pulsating water jet (UPWJ) drilling. Specifically, there is a need to explore the basic effects of varying ultrasonic technological conditions, such as traverse speed (v) vs. number of cycles and increments towards the surface. So far extensive research on using ultrasonic pulsating water jets for disintegration, surface treatment, or peening applications has been carried out or found in the open literature. However, very limited study (Mitchell et al., 2024) have been conducted related to the application of PWJ in drilling operations. The study explores the effect of circular trajectories on the potential drilling process using the PWJ method. The experiment involved creating circular paths over the sample to achieve a circular erosion shape. These trajectories were executed with different repetitions: 10, 15, and 20 times over the sample at velocities of 3 and 5 mm/s. This approach allows us to characterize the gradual material removal process and identify the key factors involved. Additionally, an 80x pass was performed to complete the drilling process, aiming to cut through the sample entirely and create a hole. The results demonstrated that the PWJ method enables targeted material division, and employing a circular trajectory can effectively achieve erosive wear of holes.

2 EXPERIMENTAL SET UP

The experiments were conducted using a device developed at the Institute of Geonics of the Academy of Sciences of the Czech Republic (Foldyna & Svehla, 2011), featuring an acoustic chamber that enhances the erosion device's effects. To achieve maximum erosion performance, i.e., material removal, the technology was tuned to resonance at a frequency (Nag et al., 2021) of 19.74 kHz and a flow rate of 1.92 l/min. The resonant frequency is important to achieve in order for the technology to operate as efficiently as possible, in converting the acoustic signal into mechanical movements. This can be achieved by changing the resistance of the water to the oscillating sonotrode. Therefore, this adjustment is performed by setting the acoustic chamber length in range 0-24 mm (Nag et al., 2019). It was found that for a given flow rate, a length of 18 mm was the most optimal length when the technology working in the resonance and impedance region. The next step is to

ensure sufficient time for the coherent water stream to transform into distinctly developed water clusters that impact the material. This adjustment is achieved by finding the optimal standoff distance at which the water clusters are formed into their integral shape. This parameter is also important because after exceeding the critical standoff distance, the integral shape of the water clusters is broken up by air resistance, thus reducing the effectiveness of the impact pressure. The standoff distance was then determined based on the maximum erosion depth using a step trajectory (Hloch et al., 2020). This optimized setup was subsequently used for technological drilling tests according to **Table 1**.

Table 1 Experimental conditions of PWJ process

Hydraulic conditions				**Technological conditions**		
p [MPa]	*d* [mm]	*Q* [l/min]	*Vw* [m/s]	*z* [mm]	*lc* [mm]	*f* [kHz]
40	0.4	1.92	254	35	18	19.74 ±0.01
Experimental conditions						
v [mm/s]		n_c	*Eh [kJ]*	*rep.*		
3		10	80.436	3x		
		15	120.654			
		20	160.872			
5		10	48.262			
		15	72.393			
		20	96.523			
2		80	965.234	1x		

The technology set up in this way was used in the main experiments to induce the drilling effect on samples of the target material AW 6060 aluminum. This material was chosen because of its promising mechanical properties, which allow monitoring of the effect on erosion depending on the change in technological parameters of the technology. A plate with a thickness of 5.5 mm was fixed with fixing screws to the table, where its upper surface was defined as zero height relative to the water jet. The optimal standoff distance was set from this base. The main experiment consisted of creating circular trajectory paths with a diameter of D = 6 mm (***Fig.1***). This diameter was chosen so that only a specific area of the point where the PWJ is located, and acts are eroded. This ensures that the erosion removes material gradually according to the trajectory in the required area, and the opposite side of the semicircle is not affected.

Due to the increasing number of passes 10, 15 and 20x cycles over the surface in a circular trajectory, the dependence on the created erosion depth was monitored (***Figure 2***). For a greater dispersion of experimental parameters, these repetitions were created at two types of traverse speed, v = 3 and 5 mm/s. Each of the experiments was repeated three times to ensure statistical significance. Due to the material thickness being too high to drill thoroughly with the selected passes. However, an additional pass was created with 80x passes over the sample. This ensured the drilling of the sample in the entire profile and the ability to analyze the resulting drilled hole. In this case, however, the feed rate was reduced to 2 mm/s, which was important for completely removing material from the center of the circle.

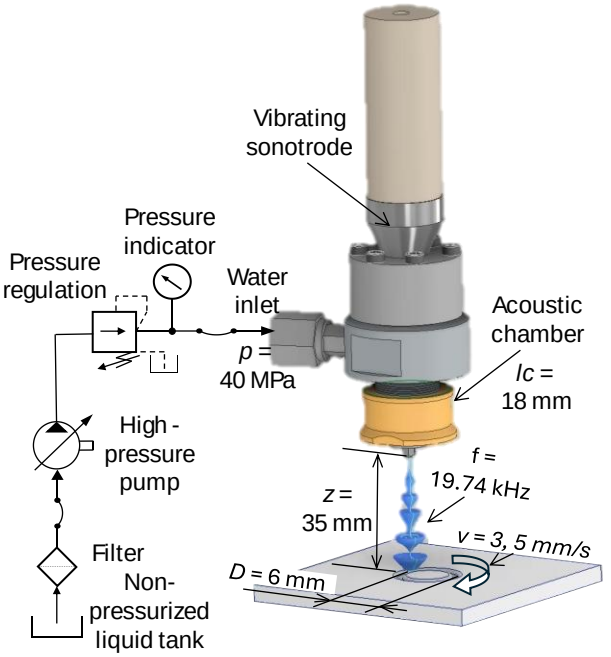

Figure 1 Experimental assembly of PWJ technology

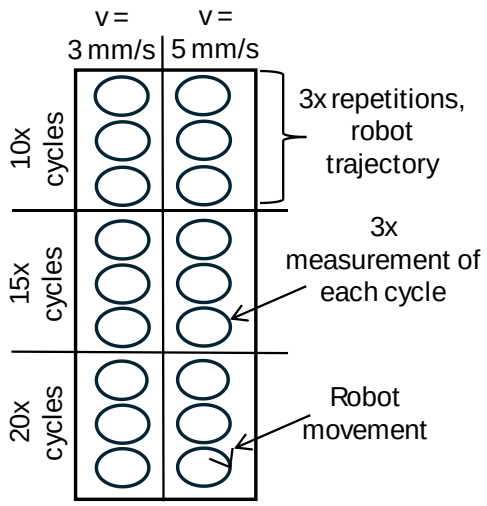

Figure 2 Hole milling experiment strategy

3 MEASUREMENT

The samples were analysed with a VHX 7000 digital microscope, which uses focal scanning to capture detailed images of the surface and allows the creation of a 3D surface map based on height differences measured according to changes in sharpness and lighting conditions. The microscope allows the analysis of key parameters of surface irregularities and the precise determination of defect dimensions. The collected data was processed into 3D visualization, which provided the possibility of detailed study and analysis of the resulting erosion traces (***Fig. 3***). In this study, only the geometry of the erosion trace, i.e. the classification of the created erosion groove, will be discussed and considered. The groove geometry itself, from the point of view of circularity, will not be considered since the inaccuracy of the positioning of the robotic arm may enter the process, which would lead to distorted and inaccurate measurement results. Furthermore, the parameters of the removed material volume and the depth of the erosion groove were analyzed together with the 3D reconstruction of the created erosion circles. The parameters of the created depth

were analyzed 5x, from which the average measured values were subsequently calculated. The threefold repetition of the experiments, together with the fivefold measurement of the depth profile of each repetition, thus provided the necessary information for graphic processing and a better display of the deviation of the created erosion and measurement.

Scans of selected samples were used to evaluate the extent and quality of erosion. These scans allow determining the extent of erosion not only from the surface but also cross-sectionally, which allows for more precise qualification of the generated erosion shape. The orientation of the cross-section was determined transversely through the created erosion circle, which allows for a comparison of erosion between the right and left sides of the sample.

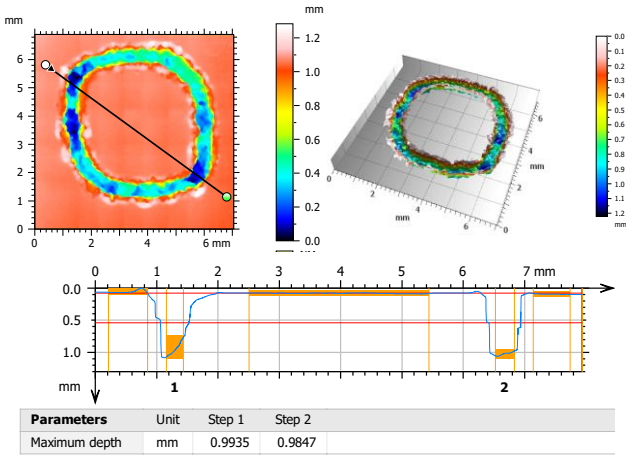

Figure 3 The strategy of measuring the created samples

4 RESULTS

4.1 Optical results

One sample from each repetition and traverse speed set was selected for optical observation of the erosion of the formed rings. This means that optical analysis compares samples after 10, 15 and 20 times of transition from each v = 3 and 5 mm/s. Selected representative scans of the samples, together with their designation, are shown in Fig. 4. It can be clearly observed that the target material was stochastically removed from the surface since the preferred orientation of the swirling was not precisely defined. This is since PWJ creates material erosion with an undefined cutting edge. This can be defined as a typical phenomenon of hydrodynamic erosion (Elhadi Ibrahim & Medraj, 2019). For this reason, after the PWJ circular drilling process, the material at the bottom of the crater is visibly roughened compared to the original and unaffected material. From this analysis, it is further evident that, in addition to forming the main erosion groove in the shape of a circle, the target material was also affected at the edge locations from the outer and inner ring rings. It is quite clear that near the erosion boundaries from the outer and inner rings of the generated circular eroded ring, the material surface is affected in the form of its cleaning and the exposure of uncontaminated underlying layers. As the number of cycles increases, this effect becomes more intense and pronounced. Therefore, it can be considered because of PWJ erosion and not as a heterogeneity of the original surface. This could be since in PWJ, water clusters are generated gradually after exiting the water nozzle. The velocity fluctuation in the vertical direction causes the transformation of the steady water jet into individual water clusters (Srivastava et al., 2021). However, these water clusters gradually expand in the lateral direction. This gradual expansion brings an uneven distribution of energy in the cross-section of the formed cluster. The largest energy should be induced in the center of the water cluster, and this energy decreases with increasing horizontal distance from the core to the periphery. This ultimately causes the central region of the water cluster to generate the highest material erosion, with the lateral parts of the generated cluster having insufficient energy to cause the same erosion effect. Therefore, the result of their action is only surface cleaning. As the number of passes increases, the loading time also increases, which also results in an increase in the surface cleaned area. It is further evident from the optical images that the stochastic removal of material caused the formation of deformed and ambiguous boundaries of the inner and outer rings. Another possible reason can be the positioning accuracy of the robotic arm to which the cutting head is attached. This inaccuracy causes an erosion groove to be formed in one cycle, but in the next cycle with a change in position, the erosion groove is widened laterally.

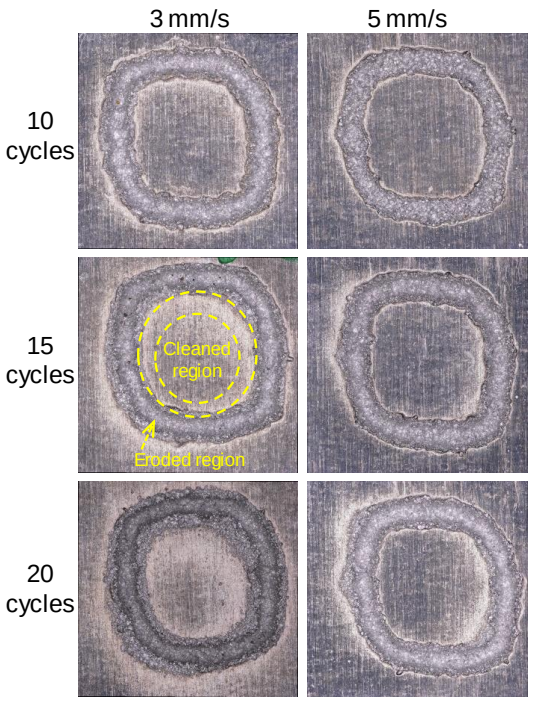

Figure 4 Optical analysis of created circular erosion

4.2 Cycle depth and volume removal

To measure the material removal, an analysis of the maximum depth was performed together with the volume of the removed material. Table 2 contains the numerical average measured values of the depth and the volume removed, depending on the number of cycles and the traverse speed. This data also contains standard deviation values, which can be used to theoretically determine the accuracy/repeatability of the process. It can be observed that as the number of repetitions increased, the rate of increase in the measured values of both depth and removed volume decreased. The depth result shows that as the impact on the material increases, it is removed, but its lower layers (depth) are deformed to approximately the same depth after each pass. This may be because during the initial stages of erosion, material is removed more rapidly due to a combination of impact pressure and lateral flow. However, with the increasing number of impacts of water clusters on a certain area, peaks and valleys are formed on the material, which creates its roughness. When a cluster of water interacts

with this roughness, its impact energy diminishes. This leads to the deformation of its overall shape and the reduction of the impact pressure, which results in a reduced erosion effect (Stolárik et al., 2023). Therefore, the bottom of the erosion crater is more difficult to erode.

Table 2 Average measured parameters of depth and removed volume

v [mm/s]	3			5		
Cycles	10	15	20	10	15	20
Depth [mm]	-0.84 ±0.06	-0.99 ±0.05	-1.20 ±0.04	-0.53 ±0.04	-0.59 ±0.03	-0.74 ±0.03
Volume [mm³]	4.45 ±0.14	5.84 ±0.06	6.97 ±0.05	2.44 ±0.14	3.30 ±0.12	4.30 ±0.09
MRR [mm³/s]	0.071± 0.0022	0.062± 0.0007	0.055± 0.0004	0.065± 0.0036	0.058± 0.0021	0.057± 0.0011

The graphical representation of the average measured values together with the error bars of the depth of the created circular grooves are shown in **Figure 5**. It is clear from the picture that with the increasing number of repetitions of individual cycles, they deepened due to the increasing load on the target material and, thus, the increasing erosion. In each case, the erosion depth was deeper for 3 mm/s compared to 5 mm/s. This can be attributed to higher material interaction time at lower traverse speed. At a v = 3 mm/s, the circular groove with the number of passes of 10 cycles was smaller by 17% compared to 15x repetition cycles. With 20x repetition, the depth was further deepened by 21% compared to 15x repetition. It follows that the depth of the circular groove was continuously enlarged, with a difference of only 4% among them. However, at a v = 5 mm/s, with a 10x repetition, the difference compared to a 15x repetition was 11%. With a 20x repetition, the difference was up to 25% compared to a 15x repetition. It is clear from this that at a v = 5 mm/s, the difference between individual depths was up to 14%. Therefore, at a v = 5 mm/s, the circular depth is less linear compared to v = 3 mm/s. This can be attributed to the fact that at a lower traverse rate, the water clusters have enough time to use their full erosion potential and thus penetrate the material more thoroughly than at v = 5 mm/s.

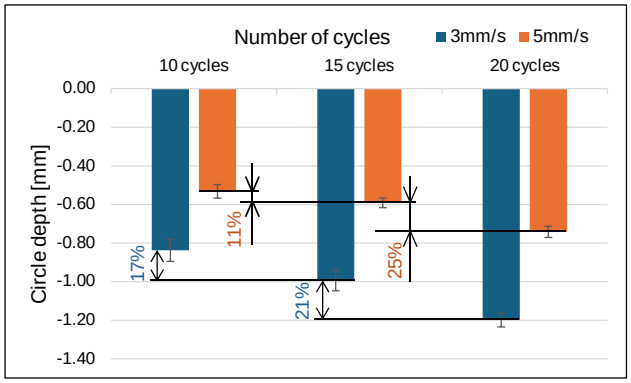

Figure 5 Comparison of the circular erosion groove depth at v = 3 and 5 mm/s

Another evaluated parameter is the average volume of material removal depending on the number of cycles and traverse speed (**Figure 6**). This parameter is also partially linked with the erosion depth discussed above. For both v = 3 and 5 mm/s, a larger volume removal was recorded with an increasing number of cycles. Furthermore, at a v = 3 mm/s, a higher rate of material removal was measured in each case than at a v = 5 mm/s. When the cycle was repeated 10 times, the volume of material removed was 45% lower at a v = 5 mm/s compared to a v = 3 mm/s. However, at 15- and 20-times repetition, this difference was gradually reduced to 43% and 38%, respectively. This result is interesting because it is unclear why such a decrease in difference was observed when all operating conditions were maintained. One of the possible explanations is that when creating a circular groove, there is a constant supply of water to the erosion site. When the erosion groove is deep enough, its lower parts are flooded with water, which is surrounded on both sides by the walls of the ring and thus has no room for its escape. This causes the accumulation of static water in the resulting space in the form of a water layer, which absorbs the energy of subsequent water clusters. However, the flooding of the lower parts of the annulus can be partially reduced by the circular trajectory work performed during the drilling process. In this case, at 5 mm/s, due to the higher speed, the water layer breaks up more often. Theoretically, at this speed, certain water clusters can be consumed to break the water surface, but this will open the way for the impact of the next cluster of water on the material and not on the water layer. In this way, the decreasing trend of the difference in the measured values of the volume of material removed can be explained.

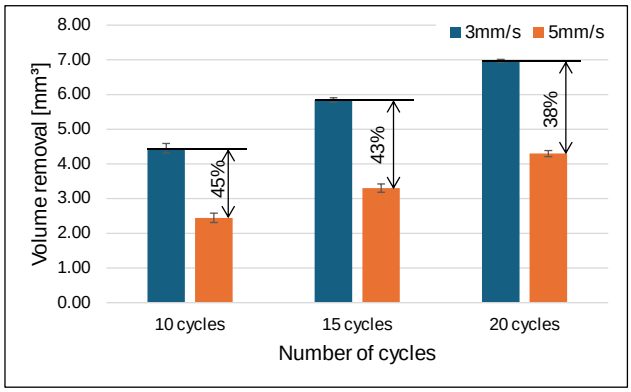

Figure 6 Comparison of removed volume of circular erosion groove at v = 3 and 5 mm/s

4.3 *Erosion characterization*

Figure 7 shows the cross-sectional view of selected circular grooves after 10-, 15- and 20-times cyclic repetition with v = 3 mm/s. This view shows the clear geometry of the rounded corners on both the inner and outer rings of the erosion walls at each cycle repeat. This phenomenon is caused by the upheaving of the water cluster and the distribution of energy in its cross-section. During the initial and first transitions, the entire load of the erosion potential of the water cluster acts on the target material of a flat surface. This causes the formation of an erosion groove with a certain width. This erosion groove is formed in a U or V shape (Fujisawa et al., 2018). However, with increasing load, erosion is constantly increasing. The highest accumulation of pressure and energy is in the axis of the water cluster. It follows that the lateral parts of the water cluster fall on the inclined walls of the U or V-shaped erosion groove which reduces the energy that could potentially be used to cause erosion by impacting the inclined wall of the material. This causes the water to partially reach the shear, and thus, the rate of erosion is reduced. In this way, an erosion profile is created, where it gradually narrows. It can also be seen that the geometry formed by 20x repetitions, characterized by the red line, prevailed over the other repetitions in the created depth. During this cycle of repetition, not only did the erosion ring deepen, but also material was pushed to the sides. This is well-observable on the right erosion groove, where the material is pushed outwards from the groove on the inner erosion ring.

However, this eroded material also has a rounded top. Therefore, it is assumed that the degree of plastic deformation occurred mainly during the initial transitions of the formation of circular grooves, and with increasing repetition, only a slight further extrusion occurred. However, with a 20x repetition, both the right and left milled grooves have a narrower character compared to the 10x transition. This diverse character could be attributed to the precision of the positioning of the robotic arm and the lateral expansion of the groove. Another possible explanation could be local material characteristics.

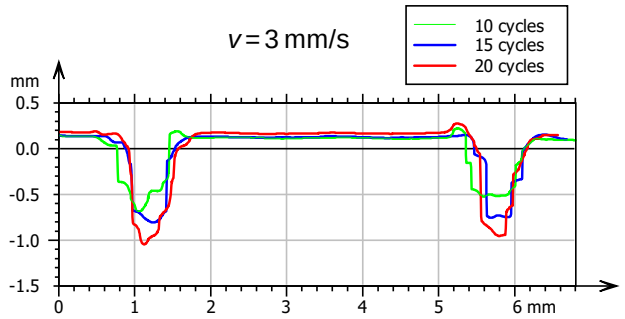

Figure 7 Transverse characterization of circular erosion at a speed of 3 mm/s

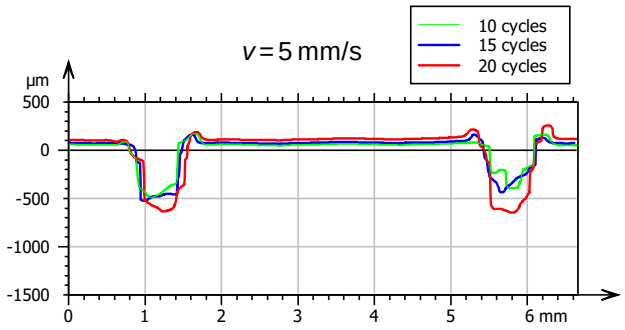

Figure 8 Transverse characterization of circular erosion at a speed of 5 mm/s

The cross-sectional view of selected circular grooves after 10-, 15- and 20-times cyclic repetition with v = 5 mm/s is shown in **Figure 8**. In this case, a significant difference can be seen compared to the previous group of circles formed at v = 3 mm/s. This difference is recorded mainly in the width of erosion circles. After 10-, 15- and 20-times repetition, the observed width is approximately the same and overlapping, with minimal differences. This means that the processes were carried out under homogeneous conditions, both from a technological and a material point of view. However, a possible explanation is a significant reduction of the material interaction compared to the v = 3 mm/s. However, in this case, plastic deformation of the corner extrusion is observed in both the left and right erosion grooves. This can be attributed to the same phenomenon as it was at v = 3 mm/s. During the initial transitions, the material was plastically deformed and pushed to the sides due to the lateral flow. However, in this case, the reduced amount of incident water clusters meant that this deformed material was not further removed. Therefore, it can be observed on several edges of the inner and outer rings of the circular erosion groove. However, it also follows from the geometry that the right side of the circular groove was more deeply eroded in comparison to the left side of the circular groove at a 20x multiple pass. This phenomenon could be explained by the technological factor of positioning the target sample.

3D visualizations of the scanned surfaces were also chosen for erosion characterization (**Figure 9**). It can be clearly observed that a deeper erosion was achieved with v = 3 mm/s compared to v = 5 mm/s, which clearly corresponds with the results of the depth formed and the volume removed. However, these images offer a broader and clearer view of the processes of the stochastic structure formed at the bottom of the erosion groove. The bottom, as well as the walls of the groove, are formed by individual peaks and valleys, which, in their connection, still have the character of deeper valleys or higher hills. Further, this characteristic changes to the erosion flank of the erosion crater for the most part. This side is formed by a rounded inner radius that transitions to a flat central surface. From the upper side, this surface is rounded to the outer radius. The walls of the central surface of the ring are homogeneously eroded. This inhomogeneity can be attributed to the formation of a wider erosion groove during the first passes due to the action of water clusters on the flat surface of the material.

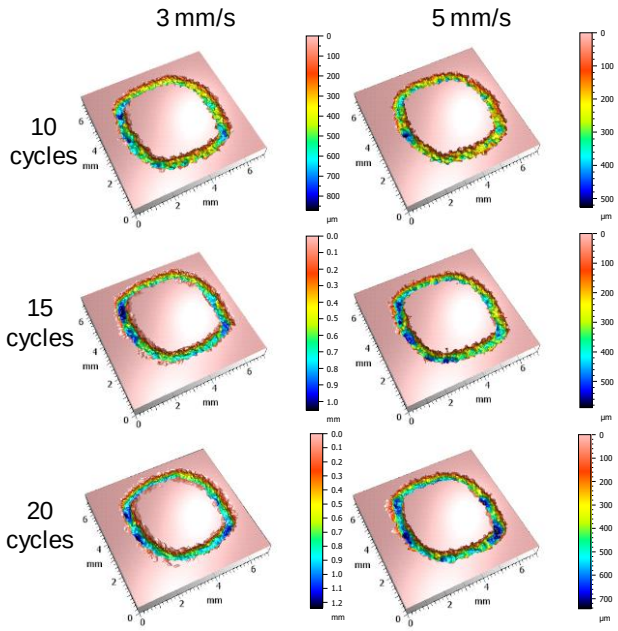

Figure 9 3D visualization of scanned surfaces of circular erosion

4.4 *Characterization of the drilled hole*

This section discusses the shape of the complete removal of the sample in a circular shape, which can be classified as a drilling process. This process was performed with 80x cycle repetitions with v = 2 mm/s. From the first glance using an optical image, the created erosion hole has a stochastic structure and deformed edges of the outer ring (**Figure 10**). In this case, it is also possible to observe the created bevel, i.e. the eroded side of the hole is not oriented perpendicular to the face but is oriented at a certain bevel angle. This can be attributed to the mentioned effect of the energy distribution in the cross-section of the water cluster. Since the highest energy, which is also associated with impact pressure, is in the centre of the cluster, this area also causes the greatest material stress and its removal. The bottom of the eroded hole has significantly deformed edges compared to the upper one. This can be explained by the process of removing the bottom of the formed groove presented in the previous chapter. Since water follows the easiest way to remove material, some areas are removed faster and more slowly, which causes the formation of a wavy bottom of the groove during the erosion process. This wavy surface may ultimately have caused a deformed and ambiguously defined edge of the ring at the bottom of the hole.

In places where there was a valley, the sample was cut earlier than in places where there was a peak. This cutting thus cleared the way for the liquid to come out from below. Since the central part of the material was in constant connection with the surrounding material, the cut groove created in the given area acted as a funnel that focused the water stream. During subsequent passes, the cut areas were additionally eroded, leading to the unification of the edge ring. However, peak areas were still only eroded from the top, and after the sample was separated, there were not enough passes for edge alignment. If additional passes were made, the central material would no longer be firmly connected to the surrounding material, preventing the creation of a focusing funnel, which directs the water stream to one spot and smooths the sides. Consequently, after the central material was separated, it was immediately pushed to the opposite side by the water clusters, which then slid along the inner and surrounding material walls. Since they weren't focused on one spot, precise focusing was not achieved, and the edge erosion was completed. A 3D visualization confirmed the chamfered edge of the side walls of the eroded material. It was observed that the walls of the milled hole were significantly inhomogeneous with roughness surface. This was confirmed with a visual photograph of the removed material. The upper part of the drilled material was chamfered, which was reduced after a depth of about one-third of the sample's total height. This indicates that lateral flow significantly affects the material up to this depth, expanding the eroded ring. Beyond this depth, the material resists due to subsequent water clusters absorbed by static water trapped at the bottom of the crater. Ultimately, the size of the annulus reduced, limiting any lateral jetting spread. As a result, the material was only removed by impact pressure. The cross-sectional characteristics of the eroded hole confirmed rounded edges on the sample's surface and a chamfered erosion course during the drilling process.

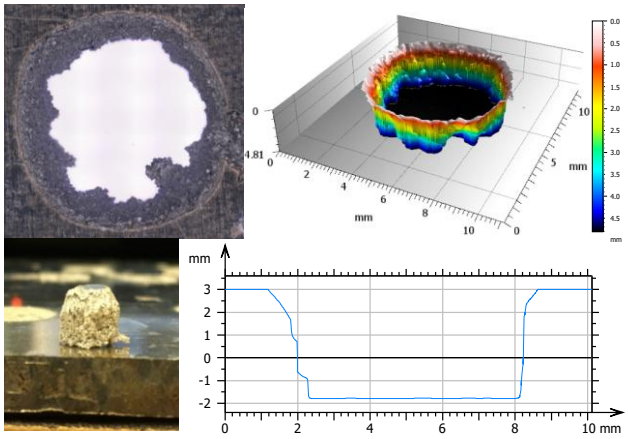

Figure 10 Visualization and characterization of a drilled hole by the circular erosion process using the PWJ method with 80x cycles repetition

These results demonstrate that a drilling process for the target material can be achieved using the PWJ method. Gradual material removal is executed through circular passes over the sample, progressively deepening it. Initially, the target material exhibits a wider erosion groove due to lateral flow, but this effect diminishes with the presence of a water layer at the bottom of the groove and the chamfered shape of the erosion edge. It was found, that the drilling wall was also significantly inhomogeneous and deformed. Therefore, it can be concluded that further finishing processes need to be considered for this material removal technology. This type of material removal could also be practically applied in industrial fields such as sandstone mining. For comparison to other technique conventional drilling method, relies on material removal using a specific cutting edge which is a solid tool and harder than the workpiece which in contrary for PWJ having no specific shape of the tool and the material hardness doesn't affect the method. PWJ doesn't provide clear or smooth drill holes but can easily be used for delicate material sensitive to the cutting forces. If compared to laser drilling, the surface finish and precision is much higher for laser drilling as compared to PWJ but limitation of the laser drilling is the material thickness and reflectivity of the material. Moreover, for heat sensitive material, both conventional drilling and laser drilling can be problematic which is advantage for PWJ being a cold cutting method. Based on these results, it is possible to extend these results to investigate circular trajectories on different types of materials in the future. This would better qualify the ability of the PWJ method to make it competitive for industrial applications. Also, different technological parameters in the form of pressure or nozzle diameter could be considered, which could theoretically lead to a more efficient process. Thus, by investigating these areas, the results could be processed for machine learning, which in this way could then help to develop control systems to have an efficient and precise technological process of material removal.

5 CONCLUSIONS

The present study shows the feasibility of utilization of PWJ as a tool for drilling applications. The main outcomes of the study are summarized as follows:

1) Increase in the cycle of repetition from 10 to 20 cycles, the mean erosion depth increased from -0.84 mm to -1.20 mm and -0.53 mm to -0.74 mm for v = 3 mm/s and 5 mm/s respectively. This increase in the circular grove depth is attributed to the increase in the impact loading of the material.
2) With lower traverse speed, the erosion depth and volume removal increase (-1.20 mm and 6.97 mm^3 for v = 3 mm/s compared to -0.74 mm and 4.30 mm^3 for v = 5 mm/s keeping 20 cycles of repetition), leading to deeper circular grooves due to longer interaction time with the material.
3) Complete drilling of the 5.5 mm thick aluminum plate was achieved using 80 cycles of repetitions with traverse speed of 2 mm/s. However, the quality of the drilled wall was stochastic which is typical for material removal by PWJ.
4) The rate of increase in the drilling depth and volume removed decreases with larger repetition due to the stagnant water layer resisting proper interaction of the water cluster with the material.
5) The deepening of the material is accompanied by chamfered edges, which can act as a funnel to focus the water cluster but prevent lateral flow erosion.
6) The accuracy of the machine positioning can influence the erosion characteristic of the transverse properties of the circular erosion grooves.

Despite the favorable results, this study was done using one workpiece material that provides an understanding of the erosion on it. For this reason, future work in this topic could concern the effect of circular trajectories on different types of

materials using different operating parameters to obtain a competitive method for material machining solutions.

ACKNOWLEDGMENTS

This study was financially supported by the Slovak Research and Development Agency under Contract No. APVV-22-0391 and Slovak Grant Agency 1/0377/22.

The experiments were conducted at the Institute of Geonics of the Czech Academy of Sciences, Ostrava-Poruba, Czech Republic, with the support for the long-term conceptual development of the research institution RVO: 68145535

REFERENCES

[Arola & McCain, 2000] Arola, D. D., & McCain, M. L. Abrasive waterjet peening: a new method of surface preparation for metal orthopedic implants. Journal of Biomedical Materials Research: An Official Journal of The Society for Biomaterials, The Japanese Society for Biomaterials, and The Australian Society for Biomaterials and the Korean Society for Biomaterials, 2000, 53(5), 536–546.

[Cook, 1928] Cook, S. S. Erosion by water-hammer. Proceedings of the Royal Society of London. Series A, Containing Papers of a Mathematical and Physical Character, 1928, 119(783), 481–488.

[Elhadi Ibrahim & Medraj, 2019] Elhadi Ibrahim, M., & Medraj, M. Water droplet erosion of wind turbine blades: Mechanics, testing, modeling and future perspectives. Materials, 2019, 13(1), 157.

[Field, J. E., 1999] Field, J. E. ELSI conference: Invited lecture liquid impact: Theory, experiment, applications. Wear, 1999, 233–235, 1–12.

[Foldyna & Svehla, 2011] Foldyna, J., & Svehla, B. Method of generation of pressure pulsations and apparatus for implementation of this method. Google Patents, 2011.

[Fujisawa, 2023] Fujisawa, K. On erosion transition from the incubation stage to the accumulation stage in liquid impingement erosion. Wear, 2023, 528, 204952.

[Fujisawa et al., 2018] Fujisawa, K., Yamagata, T., & Fujisawa, N. Liquid droplet impingement erosion on groove roughness. Nuclear Engineering and Design, 2018, 330, 368–376.

[Gujba, A. K. et al., 2016] Gujba, A. K., Hackel, L., Kevorkov, D., & Medraj, M. Water droplet erosion behaviour of Ti-6Al-4V and mechanisms of material damage at the early and advanced stages. Wear, 2016, 358–359, 109–122.

[Hancox & Brunton, 1966] Hancox, N. L., & Brunton, J. H. The Erosion of Solids by the Repeated Impact of Liquid Drops. Philosophical Transactions of the Royal Society of London. Series A, Mathematical and Physical Science, 1966.

[Heymann, F. J., 1968] Heymann, F. J. On the shock wave velocity and impact pressure in high-speed liquid-solid impact., 1968

[Hloch et al., 2024] Hloch, S., Poloprudsky, J., Siska, F., Babinsky, T., Nag, A., Chlupova, A., & Kruml, T. Erosion development in AISI 316L stainless steel under pulsating water jet treatment. Engineering Science and Technology, an International Journal, 2014, 50, 101630.

[Hloch et al., 2020] Hloch, S., Srivastava, M., Nag, A., Muller, M., Hromasova, M., Svobodová, J., Kruml, T., & Chlupová, A. Effect of pressure of pulsating water jet moving along stair trajectory on erosion depth, surface morphology and microhardness. Wear, 2020, 452–453, 203278.

[Mann & Arya, 2003] Mann, B. S., & Arya, V. HVOF coating and surface treatment for enhancing droplet erosion resistance of steam turbine blades. Wear, 2003, 254(7–8), 652–667.

[Marzbali, et al., 2023] Marzbali, M., Yeganehdoust, F., Ibrahim, M., Tarasi, F., & Jadidi, M. Liquid–Solid Impact Mechanism, Liquid Impingement Erosion, and Erosion-Resistant Surface Engineering: A Review. Coatings, 2023, 13(3), 577.

[Nag et al., 2019] Nag, A., Hloch, S., Cuha, D., Dixit, A. R., Tozan, H., Petru, J., Hromasova, M., & Müller, M. (2019). Acoustic chamber length performance analysis in ultrasonic pulsating water jet erosion of ductile material. Journal of Manufacturing Processes, 2019, 47, 347–356.

[Nag et al., 2021] Nag, A., Stolarik, G., Svehla, B., & Hloch, S. Effect of Water Flow Rate on Operating Frequency and Power During Acoustic Chamber Tuning. Advances in Manufacturing Engineering and Materials II: Proceedings of the International Conference on Manufacturing Engineering and Materials (ICMEM 2020), 21–25 June, 2021, Nový Smokovec, Slovakia, 142–154.

[Nastic et al., 2023] Nastic, A., Vijay, M., Tieu, A., & Jodoin, B. High speed water droplet impact erosive behavior on dry and wet pulsed waterjet treated surfaces. Physics of Fluids, 2023, 35(5).

[Mitchell et al., 2024] Mitchell, B. R., Korkolis, Y. P., & Kinsey, B. L. Erosion characteristics of water droplet machining. *Journal of Materials Processing Technology*, 2024, *327*, 118359.

[Poloprudsky et al., 2024] Poloprudsky, J., Gamanov, S., Chlupova, A., Klichova, D., Nag, A., Stolarik, G., & Hloch, S. Water droplet erosion assessment in the initial stages on AISI 316 L using kernel average misorientation. Tribology International, 2024, 191, 109165.

[Siahpour et al., 2023] Siahpour, P., Amegadzie, M. Y., Tieu, A., Donaldson, I. W., & Plucknett, K. P. Ultrasonic pulsed waterjet peening of commercially-pure titanium. Surface and Coatings Technology, 2023, 472.

[Srivastava et al., 2022] Srivastava, M., Hloch, S., Krejci, L., Chattopadhyaya, S., Gubeljak, N., & Milkovic, M. Utilizing the water hammer effect to enhance the mechanical properties of AISI 304 welded joints. The International Journal of Advanced Manufacturing Technology, 2022, 119(3), 2317–2328.

[Srivastava et al., 2021] Srivastava, M., Nag, A., Chattopadhyaya, S., & Hloch, S. Standoff Distance in Ultrasonic Pulsating Water Jet. Materials, 2021, 14, 88.

[Stolarik et al., 2024] Stolarik, G., Klichova, D., Poloprudsky, J., Chlupová, A., Nag, A., & Hloch, S. Submerged surface texturing of AISI 304L using the pulsating water jet method. Archives of Civil and Mechanical Engineering, 2024, 24(4), 207.

[Stolarik et al., 2023] Stolarik, G., Klichová, D., Poloprudský, J., Nag, A., & Hloch, S. Assessment of surface irregularities created by controlled liquid droplet on the surface of stainless steel AISI 304L. Engineering Science and Technology, an International Journal, 2023, 47.

[Stolárik et al., 2023] Stolarik, G., Svobodova, J., Klichova, D., Nag, A., & Hloch, S. Titanium surface roughening with ultrasonic pulsating water jet. Journal of Manufacturing Processes, 2023, 90, 341–356.

[Szada-Borzyszkowska et al., 2024] Szada-Borzyszkowska, M., Kacalak, W., Banaszek, K., Pude, F., Perec, A., Wegener, K., & Królczyk, G. Assessment of the effectiveness of high-pressure water jet machining generated using self-excited pulsating heads. The International Journal of Advanced Manufacturing Technology, 2024.

[Vijay et al., 2018] Vijay, M. M., Foldyna, J., & Remisz, J. Ultrasonic modulation of high-speed water jets. In Geomechanics, 2018, 93 (pp. 327–332). Routledge.

CONTACTS:

Ing. Gabriel Stolarik
Faculty of Manufacturing Technologies TUKE with a seat in Prešov, Slovak Republic, DEPARTMENT OF AUTOMOBILE AND MANUFACTURING TECHNOLOGIES
Bayerova 1, 080 01 Presov, Slovakia
gabriel.stolarik@tuke.sk, https://fvt.tuke.sk/